ACETANILIDE-MEDIATED FORMATION OF BRANCHED GOLD NANOPARTICLES FOR PHOTOTHERAPEUTIC APPLICATIONS IN CANCER TREATMENT

[1] Suresh Sistu, [2]Dr. Divya Gairola
[1]Research Scholar, [2]Supervisor
[1-2] Department of Chemistry, Arunodaya University, Itanagar, Arunachal Pradesh, India

Abstract

Gold nanoparticles of diverse sizes and shapes were synthesised in an aqueous solution via a one-pot preparation technique utilising acetanilide and its derivatives at a temperature of 95 °C. These molecules serve dual purposes as reducing and structural agents, facilitating the creation of branched, multibranched, and spherical gold nanostructures. The substitution at the para positions in acetanilide, including p-hydroxy and p-aminoacetanilides, results in the formation of both spherical and multibranched gold nanoparticles. In contrast, acetanilide alone leads to the exclusive production of well-controlled branched gold nanostructures. Consequently, the resulting branched gold nanoparticles can be effortlessly separated and refined without the need for complex purification methods. Remarkably, this branched gold nanostructure demonstrated enhanced structural stability over the course of a year when compared to acetanilide derivatives that facilitated branched and multi-branched gold nanostructures. The branched gold nanoparticles exhibit robust surface plasmon resonance absorption within the near-infrared spectrum. Consequently, this inspired us to utilise branched gold nanoparticles as photothermal agents in the treatment of cancer. Our experimental findings suggest that acetanilide-stabilized branched gold nanoparticles demonstrated superior photostability when compared to its derivative-stabilized gold nanostructures. The efficiency of photothermal transduction reached an impressive 62.8% when exposed to an 808 nm laser diode, significantly surpassing that of other gold nanostructures and composite materials. Specifically, in vitro studies demonstrate that the branched gold nanostructures exhibit minimal cytotoxic effects, along with efficient photothermal ablation of breast cancer cells utilising an 808 nm NIR laser.

Keyword: Acetanilide-Mediated Formation, Branched Gold Nanoparticles, Phototherapeutic, Cancer Treatment

1. Introduction

Plasmonic metal nanoparticles (NPs) have generated significant enthusiasm owing to their unique physical and chemical characteristics, especially their captivating optical features, catalytic performance, surface-enhanced Raman spectroscopic signatures (SERS), and promising applications in the biological realm, including biosensors, diagnostics, and photothermal therapy.[1-3] The dimensions, form, and material makeup of nanostructures significantly influence these characteristics. Gold nanoparticles with a variety of shapes have been utilised to create rods, cubes, plates, flat triangles, branched structures, hollow forms, and star-shaped nanoparticles.[4-6] Experimental and theoretical analyses indicate that non-spherical nanoparticles exhibit superior catalytic and SERS performance compared to their spherical counterparts, attributed to the anisotropic distribution of the electromagnetic field near the tips of the branched particles.[7] The diminutive radii at the ends of the tips of the branching or star-shaped gold nanoparticles enhance the electromagnetic field without the necessity for particle clustering. Within the visible and near-infrared spectra, anisotropic gold nanoparticles exhibit numerous plasmon resonances that are significantly influenced by polarisation. The extensive application of branched gold nanoparticles across multiple sectors in the past ten years has led to a multitude of investigations focused on the fabrication of these nanoparticles in diverse dimensions and forms. Gold nanoparticles with branched structures can be synthesised through numerous methods. The seeded growth approach stands out as the most favoured synthesis technique.[8-10] The procedure involves generating minuscule nanoparticles, whose surfaces enhance the growth within a metal ion solution, ultimately yielding the intended branched gold nanoparticles, as suggested by the terminology. A variety of elements impact morphology. The initial element involves the application of a surfactant or capping agent onto a particular facet to restrain its development and initiate a disruption of symmetry. The pace at which gold is diminished is influenced by the reducing agent involved. The selection of a reductant or a combination of reductants influences the morphology of gold nanoparticles, in addition to the reactivity of the gold ions. Additionally, foreign ions, like silver ions, can accelerate the growth of anisotropic gold nanoparticles. The presence of silver on the exterior of gold nanoparticles

hinders the continued growth of gold, attributed to the surface blocking effect, which promotes the formation of irregular shapes.[11-12] A variety of methods have been employed in the past to refine the structure of branching gold nanoparticles, irrespective of their shapes or optical characteristics. However, the stability, duration, and intricacy of these treatments have constrained their practical use.

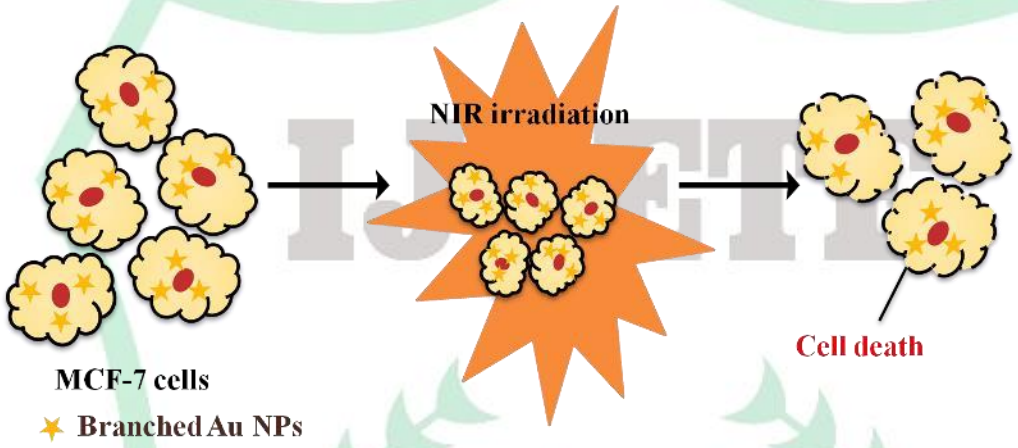

The synthesis of branching gold nanoparticles without seeds is a more uncomplicated process compared to the seeded growth method, and the majority of seedless techniques can typically be executed within a single container. The process of seedless synthesis is influenced by the same elements that dictate seeded synthesis. A specific reagent that can function as both a reducing agent and a surface capping agent is commonly employed in the seedless method. Jena and colleagues utilised 5-hydroxyindole-3-acetic acid (HIAA) as a reagent for shape control in the synthesis of marigold-like gold nanoparticles. The reagent served both as a reducing agent and as a surfactant that controls shape. A further factor influencing morphology in this research is the amount of surfactant present. To control the morphology of gold nanoparticles and diminish the presence of gold ions. Xie and colleagues utilised a biocompatible pH buffering solution composed of 2-[4-(2-hydroxyethyl)-1-piperazinyl] ethanesulfonic acid (HEPES) to synthesise branching gold nanocrystals. HEPES additionally maintains the structure of asymmetric gold nanoparticles, inhibiting their transformation into symmetric gold nanoparticles. Bakr and colleagues15 showcased a two-phase synthesis process that utilised H2O2 as a reducing agent to create spherical particles. This was succeeded by the incorporation of a thiolated capping agent, resulting in the formation of nanourchin-like gold nanoparticles. Gold nanoparticles in the shape of stars can be synthesised without seeds by utilising ascorbic acid as a reducing agent and cetyltrimethylammonium bromide (CTAB) as a stabilising agent, similar to the process used for gold nanorods. While the seedless synthesis presents an uncomplicated method for producing branching gold nanoparticles, it does come with notable disadvantages. Initially, the process that generates branched gold nanoparticles consistently results in nanoparticles with unwanted shapes in the solution, complicating the centrifugation needed to separate the desired nanoparticles. Furthermore, the optical characteristics of nanoparticles are intrinsically linked to their morphology, and the combination of different nanoparticles would expand the absorption spectrum, complicating the ability to adjust the absorption range. Ultimately, due to the high cytotoxicity of the surface capping agent, like CTAB, completely eliminating it from the nanoparticles proves challenging, requiring multiple washings or other rigorous treatments. The stability of the asymmetric gold nanoparticles is relatively low. Under standard temperature conditions, the multipod gold nanoparticles exhibit a tendency to rearrange themselves into thermodynamically advantageous spherical nanoparticles. These challenges restrict the range of optical and biological uses.

Creating innovative one-pot seedless synthetic methods for producing branched Au nanoparticles that exhibit excellent uniformity and a tight distribution, utilising new green directing and stabilising agents, presents a challenging endeavour. These NP synthesis methods are characterised by their ability to produce a diverse array of NP morphologies utilising small organic functional molecules.[16-17] These substances can additionally function as stabilising agents, facilitating the controlled development of Au NPs owing to their inherent properties. A variety of reducing agents have demonstrated the ability to alter the morphology of Au NPs by influencing the interactions and kinetics of the reaction.[18] In this context, we have recently disclosed that acetanilide serves as a shape-directing, stabilising, and reducing agent in the synthesis of branched Au nanoparticles. The interactions between reducing agents and Au precursors, along with nanoparticles, significantly influence the development of anisotropic

morphology. Reducing agents containing nitrogen functionalities, for instance, can demonstrate NAu interactions that are detectable through Fourier Transform Infrared (FTIR) spectroscopy.[19]

2. Experimental Section

2. 1. Materials: Hydrogen tetrachloroaurate (HAuCl4, 99.99%; sourced from Alfa-Aesar), Acetanilide, p-Hydroxyacetanilide, and p-Aminoacetanilide (99.5%, obtained from Merck) were utilised as received, without any additional purification steps. All experiments utilised Milli-Q grade water. All glassware was thoroughly cleaned using a non-ionic detergent, subsequently treated with Aqua regia, and rinsed with Milli-Q water before use.

2. 2. Synthesis of Branched Gold NPs: Gold nanoparticles with various morphologies were synthesised by modifying our previously published methods.20 29.5 mM of Acetanilide along with its derivatives, p-Hydroxy and p-Aminoacetanilides, were introduced into vials that held 10 mL of water. Following the dissolution of these compounds at a temperature of 95 °C, an addition of 20 µL of HAuCl4 (40 µM) was performed. The observed colour transitions shifted from a pale yellow to a bluish-grey, followed by pink and a brownish hue, respectively, after a duration of five minutes. The molar ratio between the concentration of acetanilide derivatives and HAuCl4 is 737 to 1, respectively. The heating process was extended for an additional 20 minutes without any stirring involved. The resulting solutions were allowed to reach room temperature for additional analysis.

2. 3. Isolation of Gold NSs: After a period of seven days, a dark bluish-grey and brown precipitate was noted in the vial that held acetanilide and p-aminoacetanilide. In contrast, the vial containing p-hydroxyacetanilide showed no signs of precipitate formation, even after several weeks had passed. Bulk precipitates were gathered from twenty vials, which were retrieved and separated by decanting the supernatant through centrifugation at 1000 rpm, followed by five washes with Milli-Q grade water. Isolated precipitates are allowed to dry at ambient temperature to yield a stable solid powder for subsequent investigations.

2. 4. Photothermal Conversion Assay: At the outset, the photothermal properties of gold nanostars derived from acetanilide and its related compounds were examined through temperature fluctuations when exposed to 808 nm near-infrared laser irradiation. The various concentrations of the synthesised branched gold nanoparticles (25, 50, 75, 100, 125 µg/mL) were subjected to NIR laser irradiation (808 nm NIR laser diode) for a duration of 30 minutes at an intensity of 2 W/cm². Subsequently, the temperature variations were monitored using a digital thermometer at one-minute intervals. Additionally, the branched gold nanoparticles were periodically exposed to an 808 nm laser (2 W/cm²) to examine the efficiency of photothermal conversion (η) and the stability of a 125 µg/mL solution of branched gold nanoparticles at a pH of 7 throughout five cycles of on/off near-infrared laser irradiation (2 W/cm², 808 nm laser), transitioning from lower to higher temperatures over a duration of 30 minutes. Subsequently, the irradiation process was halted and allowed to cool to ambient temperature.[24]

2. 5. Cell Culture: The MCF-7 cell line, which is derived from breast adenocarcinoma, along with the NIH 3T3 cell line, originating from mouse embryonic fibroblasts, were obtained from the National Centre for Cell Sciences (NCCS) located in Pune, India. The cell lines were cultured in Dulbecco's modified Eagle's medium (DMEM, Sigma-Aldrich), enriched with 10% (v/v) foetal bovine serum (FBS) and 1% penicillin-streptomycin solution (Sigma-Aldrich, USA), maintained at 5% CO2 in a humidified incubator set to 37°C. 7-dichlorofluorescin diacetate (DCFH-DA), phosphate buffer saline (DPBS) powders, acridine orange (AO), and ethidium bromide (EtBr) were obtained from Sigma-Aldrich, USA, and SRL, India, respectively.

2. In Vitro Cell Based Assays: In the investigation of cell cytotoxicity, the MTT-based colorimetric assay was utilised to measure the cytotoxic capabilities of acetanilide-functionalized branched gold nanoparticles. The study involved the selection of two distinct cell lines: the breast cancer cell line MCF-7 and the normal cell line NIH 3T3. The viability of the cells was assessed by determining the proportion of living cells subjected to different solutions of branched gold nanoparticles. In summary, MCF-7 and NIH 3T3 cells were plated at a density of 5000 cells per well in 96-well plates and incubated for 24 hours in triplicate. Subsequently, the cell medium was substituted with new MEM medium infused with branched gold nanoparticles and allowed to incubate for a duration of 24 hours. Untreated healthy NIH 3T3 and MCF-7 cells served as the negative control. Upon completion of the specified incubation period post-treatment, the medium was carefully discarded, and the cells underwent a gentle wash with PBS to eliminate any traces of residual branched gold nanoparticles. Each well received 10 µL of MTT dye (with a stock concentration of 5 mg/mL) and was incubated for a duration of 3 to 4 hours in a 5% CO2 environment at 37 ºC to facilitate the

development of purple insoluble formazan crystals. After the treatment, the incubation medium was substituted with 100 µL of DMSO for each well to dissolve the insoluble formazan crystals. The resulting colour intensity was assessed by measuring the absorbance at 570 nm with a microplate reader (Cytation3, Biotek). Each absorbance measurement was conducted in pairs, and the percentage of cell viability was determined using the provided formula:

Cell viability (%) = [A_{570} treated cells/A_{570} control cells] × 100

2. 7. In Vitro Photothermal Therapy: Two sets of 5000 MCF-7 and NIH 3T3 cells per well were plated in DMEM medium within 24-well plates and allowed to incubate until they achieved sub-confluence. At 70-75 % confluence, the DMEM medium was replaced with the MEM medium containing different concentrations of the branched gold NPs under standard cell culture environment. Following the designated incubation durations, the cells were exposed to varying doses of monochromatic light emitted from a source operating at 700 nm and 150 W. The spacing between the light source and the surface was fine-tuned to ensure that the cells received a consistent illumination. The energy density (J/cm2) for the application has been initially elucidated, and from this, the necessary duration for light exposure was derived using the subsequent general formula: Energy density, measured in joules per square centimetre (J/cm^2), is calculated by multiplying power density, expressed in watts per square centimetre (W/cm^2), by the duration in seconds (sec). Following NIR illumination for the designated time frame, the treated cell culture plates were subsequently incubated for varying durations in a 5% CO2 chamber maintained at 37 ºC. Following the specified duration, the cells underwent MTT assay, consistent with the procedures employed for cytotoxicity evaluations.

2. 8. Effect of Cellular Uptake on Photothermal Efficacy of Branched Gold NPs: To evaluate the impact of NIR radiation on varying cell uptake durations for branched gold nanoparticles, the cells were plated at a density of 5000 cells per well in a 24-well tissue culture plate. Once the cells reached approximately 70% confluence, they were treated with gold nanoparticles following the same protocol outlined in the in-vitro photothermal therapy assay. The cells were subsequently incubated for different durations with the nanoparticle before exposure to NIR, specifically for 1.5, 8, 12, and 24 hours. Subsequently, the cells were subjected to NIR exposure to investigate the influence of uptake duration on photothermal therapy.

2. 9. Microscopy Methods for Observation of Cellular Morphology Changes: Acridine orange–Ethidium bromide (AO–EB) Staining: MCF-7 cells exposed to different concentrations of gold nanoparticles underwent AO-EB dual dye staining to identify the occurrence of apoptotic cell death. In this experiment, 5000 MCF-7 cells per well were plated in 6-well cell culture plates and subsequently exposed to the specified concentrations of nanoparticles for a duration of 24 hours. Following the incubation phase, the MEM medium was carefully aspirated, and the treated cells underwent a wash with ice-cold PBS. The cells were subsequently treated with a mixture of AO-EB dye at a working concentration of 10 µg/mL for a duration of 15 minutes at a temperature of 37 ºC. The fluorescent images were subsequently captured using various filters available with an inverted fluorescent microscope (EVOS® FL Colour, AMEFC 4300).

2. 10. Evaluation of Change in Mitochondrial Membrane Potential (MMP, Δψm):

The alteration in mitochondrial membrane polarisation (MMP, Δψm) was assessed by observing the fluorescence quenching of the lipophilic dye rhodamine 123 (Rho 123). In order to examine the alteration in MMP, 10,000 MCF-7 cells per well were plated in a 6-well dish and cultured until they reached sub-confluence. Subsequently, they were treated with different concentrations of branched gold nanoparticles and then subjected to NIR exposure for a duration of 8 hours. Following the incubation period, the cells underwent a washing process using ice-cold PBS, after which they were subjected to further incubation in ice-cold PBS containing a concentration of 5 µg/mL of Rho 123. The cells exposed to different concentrations of branched gold nanoparticles (5 µg/mL, 10 µg/mL, and 25 µg/mL) were incubated at 37 °C for 30 minutes in a dark environment, maintained at 37 °C with 5% CO2 under humidified conditions. Following the established incubation period, the cells were rinsed with ice-cold PBS and examined using an inverted fluorescence microscope fitted with a range of filters.

2. 11. Evaluation of Oxidative Stress in Nanoparticle Treated and NIR exposed Cells: Considering that gold nanoparticles can independently cause oxidative stress, there remains a potential for oxidative stress induction as a consequence of the photothermal effect. Therefore, it is crucial to assess the oxidative stress elicited by NIR-treated branched gold nanoparticles. A total of 10,000 MCF-7 cells per well were plated in 6-well cell culture plates and cultivated until they reached confluence. The cells were subsequently exposed to varying concentrations of branched

gold nanoparticles for a duration of 6 hours. Subsequently, the cells underwent photothermal therapy using NIR light for a duration of 60 seconds and were then placed in cell culture conditions for an additional 6 to 8 hours. The medium from the cells treated with NIR exposed NPs was subsequently aspirated, and the cells were rinsed with 200 µL of PBS buffer. This was followed by the application of 20 µM non-fluorescent DCFH-DA dye to the cells for a duration of 20 minutes, after which they were incubated at 37 ºC in dark cell culture conditions. The DCFH-DA is utilised to assess the level of ROS production within the cells. Following the dispersion of dye throughout the cells, the acetate groups are cleaved by intracellular esterase enzymes found within the cells. Consequently, DCFH-DA is transformed into the intensely fluorescent compound 2,7-dichlorofluorescein (DCF) through the process of oxidation. DCF exhibits peak excitation and emission wavelengths at 495 nm and 529 nm, respectively. After the incubation period, the samples that underwent treatment were analysed for DCF fluorescence using an inverted fluorescence microscope that was fitted with a range of filters.

2. 12. Statistical Analysis:

The values from the experimental data are represented as mean ± standard error of the mean (SEM) across all experiments conducted. The data points underwent analysis using Student's t test or two-way ANOVA, incorporating various comparison techniques depending on their applicability, facilitated by the software Graph Pad Prism 0. Statistically significant values are represented as ns = non-significant, *($p < 0.05$), **($p < 0.005$), and ***($p < 0.001$).

2. 13. Characterization Techniques: The UV-visible spectra for the samples were obtained utilising a Varian Cary 100 Bio Dual beam spectrophotometer, covering a wavelength range from 190 to 1100 nm. The analysis via transmission electron microscopy (TEM) was conducted utilising FEI, TF30-ST apparatus functioning at an acceleration voltage of 300 kV. The TEM specimens of gold solutions, utilising various derivative-mediated acetanilide, were created by depositing a droplet of liquid onto a carbon-coated copper grid (400 meshes), subsequently allowing the solvent to evaporate at ambient temperature. The analysis of branched GNPs was conducted using inductively coupled plasma-optical emission spectrometry (ICP-OES) with the Perkin Elmer Optima 5300 DV, utilising standard calibration samples. The X-ray diffraction analysis of branched gold nanoparticles was conducted utilising Bruker D8 Advance instruments, employing a Cu, Kα source with wavelengths of 1.5406 Å in thin film mode.

3. Results and Discussion

Acetanilide along with its derivatives, such as p-hydroxyacetanilide, exhibited limited solubility in water-based solutions. Under increased temperatures, these molecules fully dissolve and interact with gold precursors, resulting in the creation of gold nanoparticles. It is noteworthy that the functional group located at the para-position of acetanilide significantly influenced the formation of gold nanoparticles. For instance, a grayish-blue hue was noted when acetanilide was present, while the colour transitioned progressively from pink to dark brown in the presence of p-hydroxy and p-aminoacetanilide, respectively. Figure 1 illustrates the photographic depiction of the colour development of gold nanoparticles in the presence of various acetanilide molecules. This may result from the nucleation rate of gold atoms as Au ions are reduced into Au atoms, which then coalesce to create gold nanoparticles. The formation of colour arises from light scattering, which is significantly influenced by the dimensions of gold particles present in the solutions. To explore the surface plasmon features of the resulting solutions, UV-visible spectroscopy was conducted. As illustrated in Fig. 2a-c, the optical spectra of the solutions exhibit a significant dependence on the colouration of the solutions. The acetanilide devoid of substituents generates two distinct peaks: one at a shorter wavelength and the other at a longer wavelength, especially within the near-infrared (NIR) spectrum. Conversely, a minor peak at 520 nm was detected in the scenario involving a p-aminoacetanilide solution that included gold nanoparticles. A broader peak emerged at 620 nm in the solution of p-hydroxyacetanilide that includes gold nanoparticles. The peaks exhibited the distinctive features of the surface plasmon resonance band associated with gold nanoparticles, which unmistakably signifies the synthesis of gold nanoparticles.Twenty-one The characteristics of the absorption spectra are significantly influenced by the dimensions and morphology of the gold nanoparticles in solution. Consequently, the detected absorption peak at various wavelengths may result from the emergence of gold nanoparticles with differing sizes and shapes. The crystalline structure of the gold nanoparticles, prepared with acetanilide and its derivatives, was examined through XRD measurements. The XRD pattern observed for these gold nanoparticles reveals the face-centered cubic (fcc) structure characteristic of gold nanoparticles, indicated by the 2θ angles at 38.6°, 44.5°, 64.5°, and 77.8° corresponding to the (111), (200), (220), and (310) planes (Fig. 2d), which are

associated with metallic gold.twenty-two It is noteworthy that a prominent (111) diffraction peak is detected across all the samples, indicating that the creation of gold nanoparticles is significantly enriched with the (111) crystalline plane. The width of the peak was noted to be greater than that of bulk metallic gold, thereby affirming the presence of gold nanoparticles in these solutions. To examine the dimensions and structure of the gold nanoparticles acquired from the solutions, transmission electron microscopy (TEM) was performed. In the earlier study, it was noted that branched gold nanoparticles were solely produced in the scenario involving uncomplicated acetanilide. The mean quantity of tips surrounding the spherical core in branching particles was determined to be 3 ± 1.3 nm. The dimensions of the tip were assessed, revealing a length of 26 ± 10 nm tenths of a millimetre and a width of 21 ± 7 nm, correspondingly. The formation of extended tips surrounding the central core of the particles can be linked to the detected red shift of the longitudinal plasmon band, which shows heightened intensity in the optical absorption spectra. Figure 3g illustrates that paminoacetanilide resulted in the formation of larger, multi-branched gold nanoparticles, measuring 32 nm in diameter.

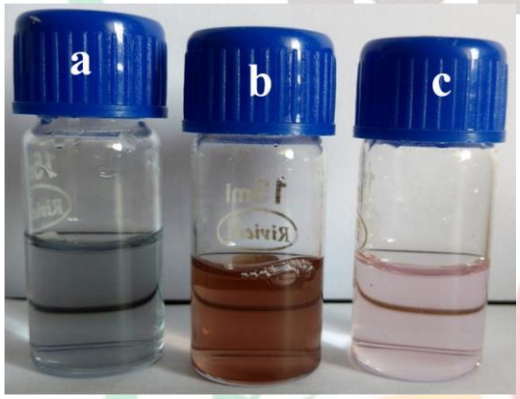

Fig. 1. *Photography indication of different colors of gold NPs using different derivatives of acetanilide (a) acetanilide, (b) p-aminoacetanilide, and (c) p-hydroxyacetanilide.*

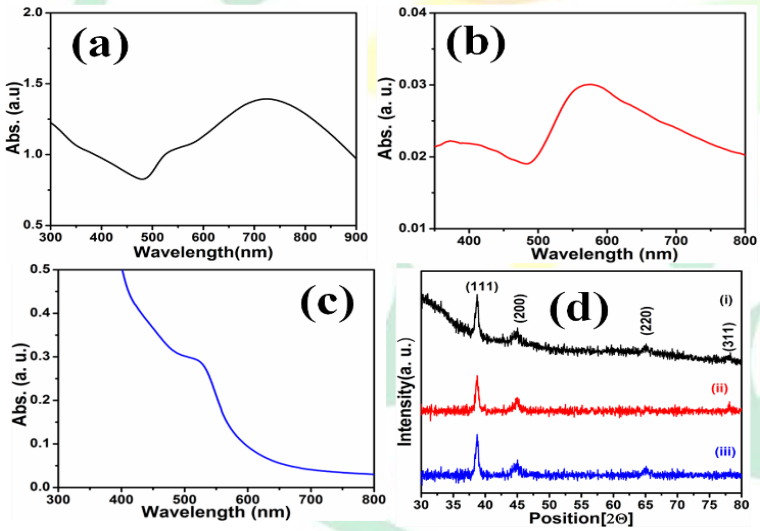

Fig. 2. *UV-visible spectra of gold NPs formed using different derivatives of acetanilide (a) acetanilide, (b) p-aminoacetanilide, and (c) p-hydroxyacetanilide and (d) their corresponding X-ray diffraction pattern respectively.*

The temperature of the gold nanoparticle solution was measured while exposed to an 808 nm laser at a power density of 2 W/cm² for a duration of 10 minutes. This was conducted to investigate the photothermal characteristics of gold nanostructures with different morphologies derived from acetanilide and its derivatives (Fig. 4, laser apparatus). The photothermal effect of ultrapure water was evaluated under identical conditions as a control sample. Figure 4a illustrates the complete array of findings. The temperature fluctuations observed in the gold nanoparticles

with p-amino and hydroxy acetanilide solutions were recorded at 52 °C and 46 °C, respectively, in contrast to the control group. In contrast, branched gold nanoparticles synthesised from acetanilide exhibited superior photothermal performance. Additionally, even at minimal concentrations (25 μg), branched gold nanoparticles demonstrated photothermal efficacy, achieving a temperature rise of 46 °C within 30 minutes of exposure to irradiation. The longitudinal absorption peak of the branched gold nanoparticles is approximately 750 nm. While the nanoparticles are optimally suited for a 750 nm laser, the 808 nm wavelength is nearer to the near-infrared spectrum. The NIR light induces a subtle auto-fluorescence and penetrates living tissues significantly, which is beneficial for medical diagnosis and therapeutic applications. In addition, the branched nanoparticles exhibit significant absorption at a wavelength of 808 nm. These inspire us to explore the photothermal phenomenon of branched gold nanoparticles synthesised from acetanilide solutions with the application of an 808 nm laser. The photothermal stability of branched gold nanoparticles is illustrated in Fig. 5a. Following five cycles of heating and cooling, achieved by alternating the NIR laser on for 30 minutes and off for another 30 minutes, a notable decline in temperature was recorded after the continuous repetition of this process across all cycles. This observation strongly demonstrates that branched gold nanoparticles exhibit superior photothermal stability compared to other gold nanoparticle morphologies derived from acetanilide derivatives. The efficiency of photothermal conversion for branched gold nanoparticles was assessed by monitoring the temperature increase over time and the energy exchange equilibrium, in accordance with the equation proposed by Roper et al.The efficiency of photothermal transduction (η) for branched gold nanoparticles (NPs) was determined using the equation (1) as referenced in sources [24, 25-27].

$$\eta = \frac{hS(T_{max} - T_{sur}) - Q_0}{P(1 - 10^{-A_{808}})} \ldots\ldots (6.1)$$

In this context, h denotes the heat transfer coefficient, S signifies the surface area of the container, Tmax indicates the peak steady-state temperature (63 °C), Tsur refers to the surrounding ambient temperature (25 °C), and Qo represents the heat released from the light absorbed by the solvent.

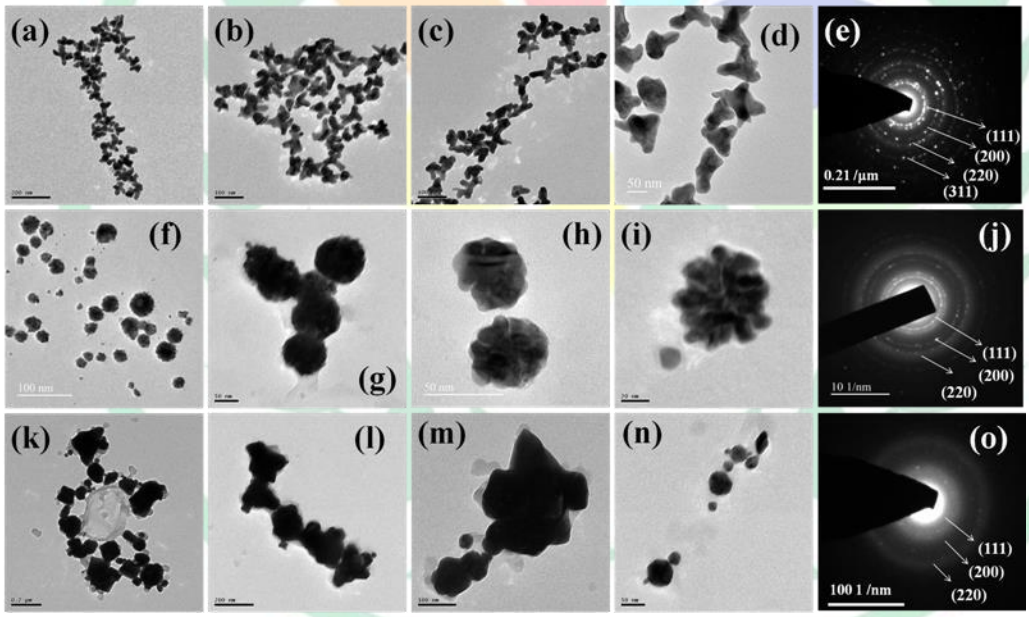

Fig. 3. *TEM and HRTEM images of branched and multi-branched gold NPs stabilized by acetanilide (a-d) acetanilide, (f-i) p-aminoacetanilide, and (k-n) p-hydroxyacetanilide and (e, j, and o) are their corresponding SAED patterns respectively.*

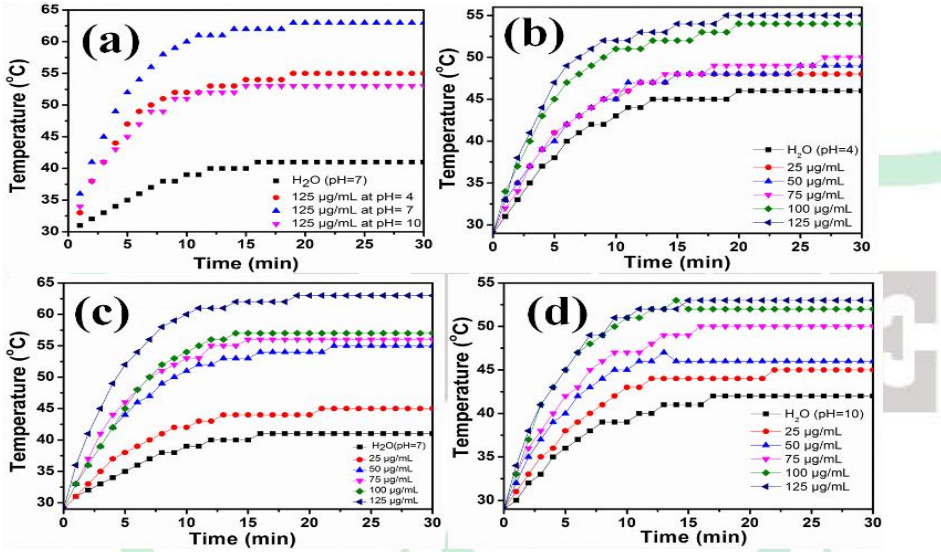

Fig. 4. *(a-d) The temperature increment versus irradiation time of the branched gold NPs at different pH under NIR irradiation for 30 min (2 W/cm^2, 808 nm laser), (a) comparison of constant concentration of branched gold NPs at pH's, (b) different concentration of branched gold NPs at pH = 4, (c) different concentration of branched gold NPs at pH = 7, (d) different concentration of branched gold NPs at pH = 10.*

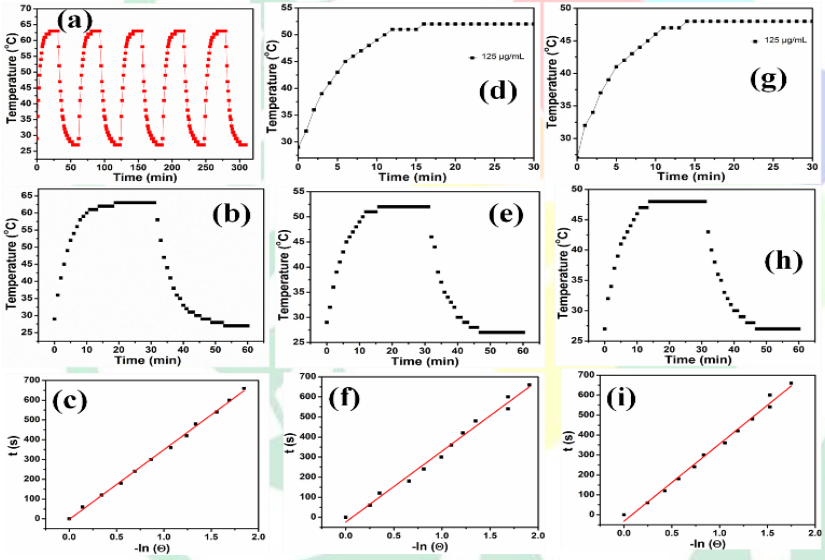

Fig. 5. *(a) photothermal stability of 125 µg/mL branched gold NPs solution at pH = 7 during the 5 cycles of on/off NIR laser irradiation (2 W/cm^2, 808 nm laser) from room temperature to top temperature, (b, e, and h) photothermal effect of the irradiation of the 125 µg/mL aqueous solution of branched gold NPs with a 2 W/cm^2, 808 nm laser. The solution is irradiated for 1800 s using a 2 W/cm^2, 808 nm laser and cooled to room temperature under ambient environment, (d, g) The temperature increment versus irradiation time of the branched gold NPs at pH = 7 under NIR irradiation for 30 min (2 W/cm^2, 808 nm laser), and (c, f and i) plot of linear fitting time data versus negative natural logarithm of driving force temperature obtained from the cooling stage (after 1800 s) of acetanilide, p-aminoacetanilide and p-hydroxyacetanilide stabilized branched and multibranched gold NPs respectively.*

and quartz sample cell, *P* is the incident laser power (2 W cm^{-2}), and A_{808} is the absorption of sample at 808 nm (0.00140).

The value of hS is derived from Equation (2):

$$\tau = \frac{m_D c_D}{\mathrm{hS}} \ldots\ldots (6.2)$$

Where τ is the time constant for heat transfer of the system which was determined to be τ = 415 from the Fig. 5f. m_D and c_D are respectively mass (125 µg) and heat capacity (4.2 $Jg^{-1}\,{}^{o}C$) of the deionized water used to disperse the gold NSs. so, the hS was determined to be

1.265 $\times 10^{-6}$ W. Q_o represents the dissipation from the light absorbed by the water and quartz sample cell, so Q_o was calculated according to the Equation (3):

$$Q_0 = \frac{m_D c_D \left(T_{\max\,(water\ )} - T_{sur}\right)}{\tau_{(water\ )}} \ldots\ldots (6.3)$$

Where, $T_{max(water)}$ is 41 ^{o}C, $\tau_{(water)}$ is 382, so, Q_o was calculated to be 0.1759 W.

The efficiency of photothermal conversion for acetanilide-stabilized branched gold nanoparticles surpasses that of their derivative-stabilized gold nanostars, as illustrated in Table 1. This pertains to the attainment of absorption maxima at 750 nm, which greatly enhances photothermal conversion efficiency. Consequently, branched gold nanoparticles exhibiting extensive near-infrared absorption render them excellent prospects for photothermal therapy, as their wide absorption spectrum (instead of a sharp, narrow one) negates the necessity for a particular laser frequency. The branched gold nanoparticles exhibited stability within a pH spectrum of 4 to 10, suggesting their enhanced suitability for application as phototherapeutics. The notably enhanced structural integrity of acetanilide-stabilized gold nanoparticles regarding pH levels, storage conditions, exposure to irradiation, and thermal stability would greatly broaden the practical applications of photothermal therapy.

Table 1. *Comparison of the Photothermal Transduction Efficiency (η) of Acetanilide and its derivatives Stabilized Branched gold NPs.*

sample	Absorbance (a. u.)	τ (sec)	η (%)
Acetanile/Branched gold NPs	0.00140	415	62.8
p-Aminoacetanile/Multi-branched gold NPs	0.00157	353	56
p-Hydroxyacetanile/Multi-branched gold NPs	0.00191	387	46

3. 1. Investigation of Cell growth Inhibition by NIR Treated Branched Gold NPs (Photothermal Effect):

Photothermal therapy has surfaced as a novel approach to cancer treatment, providing a targeted method for the destruction of tumour cell clusters. This specific form of cancer treatment is accomplished by transforming light into thermal energy, resulting in the heat-induced destruction of cells via the light-absorbing nanomaterials present within them. Consequently, the synthesised branched gold nanoparticles were evaluated for their efficacy in combating cancer cells. While gold nanoparticles are recognised for their biocompatibility, the potential cytotoxic effects of the synthesised nanoparticles were investigated using the MTT-based cell cytotoxicity assay on both normal NIH 3T3 cells and breast cancer-specific MCF-7 cells in vitro (Fig. 6 and 8). Our observations revealed that there was no significant cytotoxicity exhibited by the nanoparticles on their own following a 24-hour incubation period, highlighting the biocompatible characteristics of the synthesised nanoparticles. Additionally, for photothermal therapy, the duration of NIR radiation exposure to the cells was fine-tuned according to the calculations of energy and power density outlined in the materials and methods section. It was observed that, in comparison to a 60-second exposure duration, a 90-second exposure to NIR with a spot surface area of 7.5 cm^2 proved to be the most effective for exposure while exerting minimal impact on the healthy untreated cells (Fig. 6 and 8). The nanoparticle exposed to NIR irradiation demonstrated a cell-killing effect that was dependent on concentration (5 µg/mL, 10 µg/mL, 25 µg/mL, 35 µg/mL), assessed over a duration of 24 hours. The investigation revealed that the nanoparticle exhibited

a significant impact, achieving an IC50 value at concentrations as low as 5 µg/mL for samples subjected to NIR irradiation. Furthermore, to gain a comprehensive understanding of the cell death induced by NIR irradiated nanoparticles, an investigation into the time-dependent uptake and photothermal effects was conducted (Fig. 7).

3. 2. Investigation of Effect of Cellular Uptake on Phothermal Efficacy of Branched Gold NPs:

In order to gain a deeper insight into how light interacts with nanoparticles within cells, the research was conducted in a time-dependent fashion. It is noteworthy that we have detected the internalisation of nanoparticles in a time-dependent fashion by directing branched gold nanoparticles to various subcellular locations, contingent upon the duration of incubation. It was observed that for a duration of up to 1.5 hours, there was no significant impact of NIR on cells treated with nanoparticles (Fig. 7). This could be attributed to the nanoparticles being located on the cell surface or their adherence to the cell membrane, as well as the timing of their internalisation into different compartments and their localisation within the perinuclear region. The highest level of cell death was noted at the 8-12 hour mark, which may be attributed to the proximity of branched gold nanoparticles to different organelles. We took this specific time-dependent effect into account to enhance the therapeutic efficacy of NIR-based branched gold nanoparticles for effective cell destruction. Our research has uncovered that the photothermal effect mediated by multi-branched gold nanoparticles is distinctly different from the conventional hyperthermia-based approach. In the latter, the temperature of the entire targeted tumour cells is raised above a specific threshold that leads to cell death. Accordingly, consistent with earlier documented findings, we expect that the branched internalisation process will occur via endosomes, followed by release (Fig. 7). The subsequent effect was notably diminished when contrasted with the 8-12 hour time intervals. This may suggest that the NIR exhibited greater efficacy when nanoparticles were positioned close to different organelles, as opposed to their uptake within the nuclear region. Our findings intriguingly align with a recent study that has sought to quantitatively assess the impact of cell death in order to enhance the therapeutic efficacy through an EtBr-based assay.[28-29] Consequently, the refined time scale for the photothermal effect offers enhanced understanding to achieve a precise clean cell death response. Therefore, in addition to gold nanoparticles, they could function as mininanobomb agents that contribute to the destruction of intracellular organelles, thereby affecting metabolism through a micro-explosive mechanism within the cells.[30] The aforementioned effect may be associated with the excitation linked to the localised surface plasmon (LSP) of gold nanoparticles, resulting in the production of short pulses within the 700-800 nm spectrum. This phenomenon consequently generates elevated temperatures, thereby inducing heat within specific subcellular regions where nanoparticles are localised within the cells. Consequently, these heat shock waves result in the impairment of cellular organelles and biomolecules within the cell compartments, ultimately leading to cellular destruction.

3. 3. Study of Any Change in Cell Morphology:

To understand the cell death induced by NIR-treated branched gold nanoparticles, the cells were stained using AO/EB fluorescent dyes, which are renowned for highlighting any nuclear alterations and the formation of apoptotic bodies that are indicative of programmed cell death (apoptosis).[31] This method is regarded as a straightforward approach to distinguish apoptotic cells from necrotic cells. The AO is a vital dye which stains live and dead cells equally whereas EB only stains dead cell which lost their membrane integrity. Living cells exhibit a green hue due to the fluorescence imparted by AO, which penetrates the cell nuclei, as illustrated in Fig. 9a. The underlying cause of the green fluorescence is the intercalation binding mode of AO with the double-stranded DNA. As a result, the cells that underwent treatment were differentiated when compared to the control cells. In contrast to the control cells that exhibited a uniform green colouration, the treated cells displayed different phases of cell death. For instance, the early apoptotic cells were characterised by bright green dots within the nucleus, indicative of chromatin condensation and nuclear disintegration, as illustrated in Fig. 9b. The cells in the late stages of apoptosis permit the permeation of EB, resulting in an orange-red fluorescence, as illustrated in Fig. 9c–f. The process responsible for the fluorescence colour of EB resembles that of AO in terms of the binding intercalation mode. Consequently, the dual staining aligns with the cytotoxicity assay, indicating a greater number of cell deaths resulting from the treatment with NIR-exposed branched gold nanoparticles.

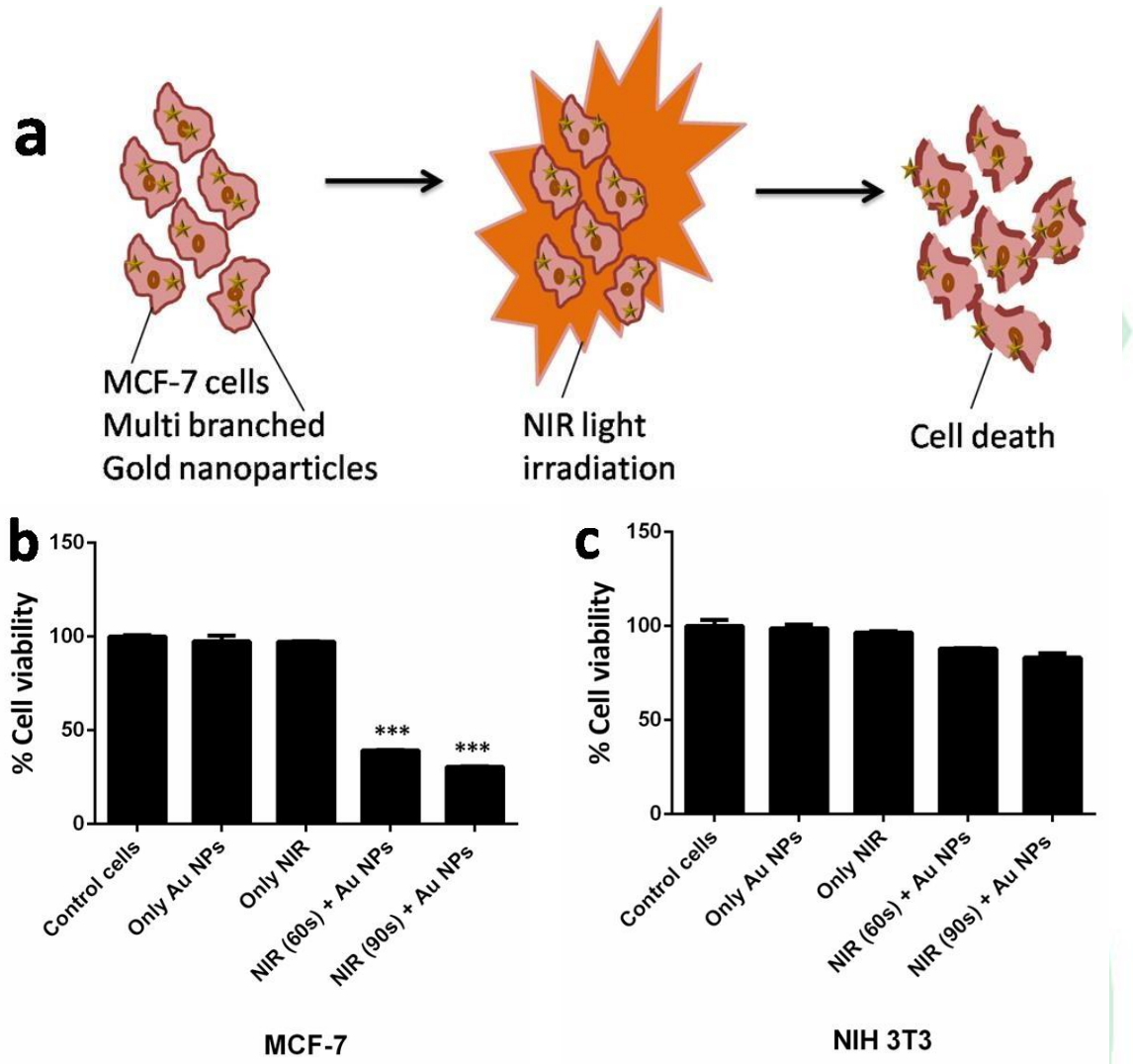

Fig. *(a) Schematic representation of photothermal effect of NIR irradiated nanoparticle treated breast cancer cells, (b) and (c) cell viability of MCF-7 and NIH 3T3 cells investigated after treatment with control cells, Only branched Au NPs, only NIR light, NIR light irradiation for 60 s with branched gold NPs and NIR irradiation time 90 s with branched gold NPs. The values are corresponding as mean ± S.E.M. (n = 2). Two-way ANOVA with Dunnett's multiple comparisons test was done to determine level of significance from the control cells. Statistical significance between different formulations are denoted by *p < 0.05, **p < 0.005, and ***p < 0.001.*

3. 4. Effect of NIR irradiated Branched Gold NPs on Mitochondrial Membrane Potential (MMP):

Mitochondria represent a crucial cellular organelle that influences the apoptotic cell death pathway. A decline in the mitochondrial membrane potential serves as a sign of initial apoptotic occurrences within the cell. To comprehend the function of mitochondria in the apoptotic process triggered by NIR treatment

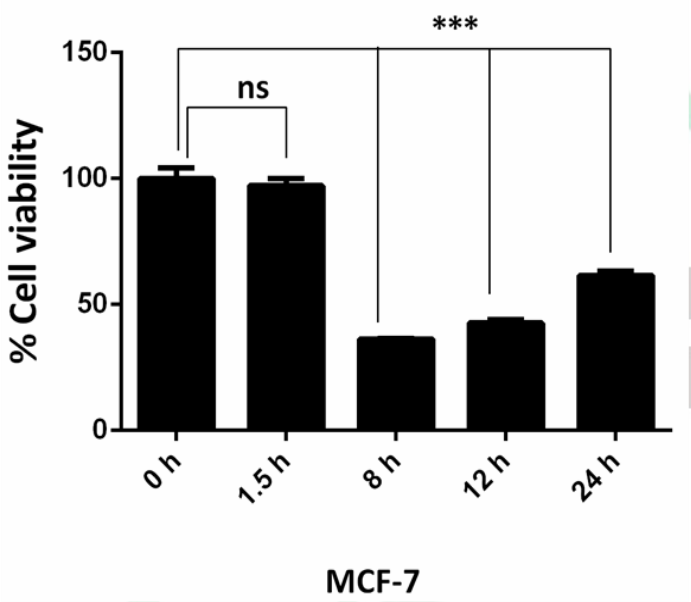

Fig. 7. *Histogram showing the photothermal effect in time dependent manner based on cellular uptake time for the nanoparticle inside the cells. The values are corresponding to as mean ± S.E.M. (n = 2). Two-way ANOVA with Dunnett's multiple comparisons test was done to determine level of significance from the control cells. Statistical significance between different formulations are denoted by ns = non significant, *p < 0.05, **p < 0.005, and ***p < 0.001.*

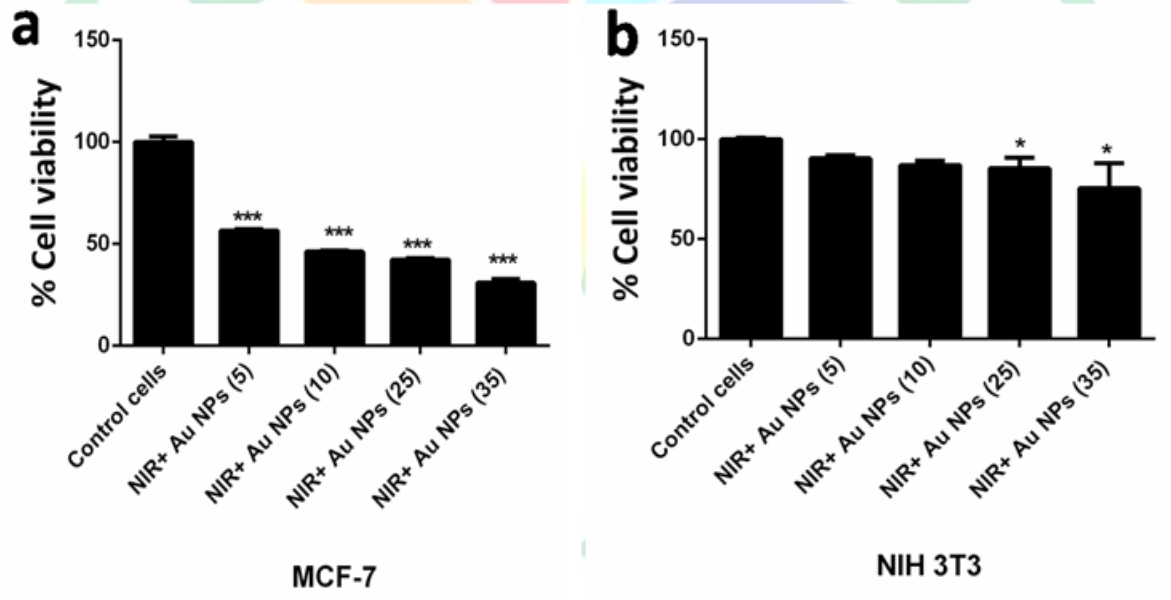

Fig. 8. *Cell viability of (a) MCF-7 and (b) NIH 3T3 cells as calculated from the MTT assay. The cells were treated with different concentration of branched gold NPs followed by NIR treatment. The values are corresponding as mean ± S.E.M. (n = 2). Two-way ANOVA with Dunnett's multiple comparisons test was done to determine level of significance from the control cells. Statistical significance between different formulations are denoted by *p < 0.05, **p < 0.005, and ***p <0.001.*

The induction of apoptosis mediated by nanoparticles involved the use of a cationic lipophilic dye known as Rho 123. It has the ability to swiftly permeate the mitochondrial matrix, influenced by the mitochondrial membrane potential

(MMP). Consequently, it can act as a marker for functional mitochondria and will be eliminated from the cells once the mitochondrial membrane potential (MMP) is diminished, leading to a reduction in fluorescence within the cells. Consequently, the alterations in mitochondrial membrane polarisation were assessed through dye-based fluorescence analysis after the introduction of branched gold nanoparticles, both with and without exposure to near-infrared light (Fig. 10a-h). In the control samples, comprising the untreated cells and those treated solely with NIR and branched gold nanoparticles, the depolarisation was assessed. It was noted that the cells exhibited a vibrant fluorescence of the dye, indicating the dye's presence within the cells, which reflects the intact mitochondrial membrane potential (MMP). Conversely, in the samples subjected to treatment with different concentrations (5 µg/mL, 10 µg/mL, and 25 µg/mL) of branched gold nanoparticles, the noticeable reduction in fluorescence of rhodamine 123 dye, compared to control cells, distinctly indicates a decrease in mitochondrial membrane permeability.Thirty-three Following 8 hours after exposure to branched gold nanoparticles, there was a significant loss of membrane polarisation observed in the MCF-7 cells. The findings indicate that alterations in the mitochondrial membrane potential (MMP) trigger a signalling cascade that activates mitochondria, ultimately resulting in the induction of apoptotic cell death. Consequently, it is essential to assess the production of reactive oxygen species (ROS) within the cells, as mitochondria are recognised for their role in triggering apoptotic signals through a ROS-mediated process, acting as a possible source of ROS generation.

3. 5. Induction of Intracellular ROS Generation in NIR Treated Cells:

Following the MMP investigation, an assessment of intracellular ROS production was conducted utilising DCFH-DA dye. Mitochondria, often referred to as the powerhouse of the cell, function as the primary locations for the generation of reactive oxygen species (ROS). Consequently, they are regarded as the principal areas where oxidative stress is triggered following damage to the organelle.[34] Our research revealed that there was a significantly reduced generation of ROS in cells treated with branched gold NPs and those treated solely with NIR, in contrast to the cells that received the combined treatment of both. Significantly, there was a substantial production of reactive oxygen species (ROS) with the rising concentration of branched gold nanoparticles following near-infrared (NIR) exposure (Fig. 11). The increase in ROS resulting from a higher concentration of branched gold nanoparticles can be attributed to the proximity of these nanoparticles to the mitochondria within the tumour. Consequently, the application of NIR produces a substantial impact, leading to considerable structural alterations that subsequently trigger the production of ROS following the photothermal effect.[35] The outcomes of ROS generation demonstrated the occurrence of intracellular oxidation during the photothermal therapy facilitated by branched gold nanoparticles.

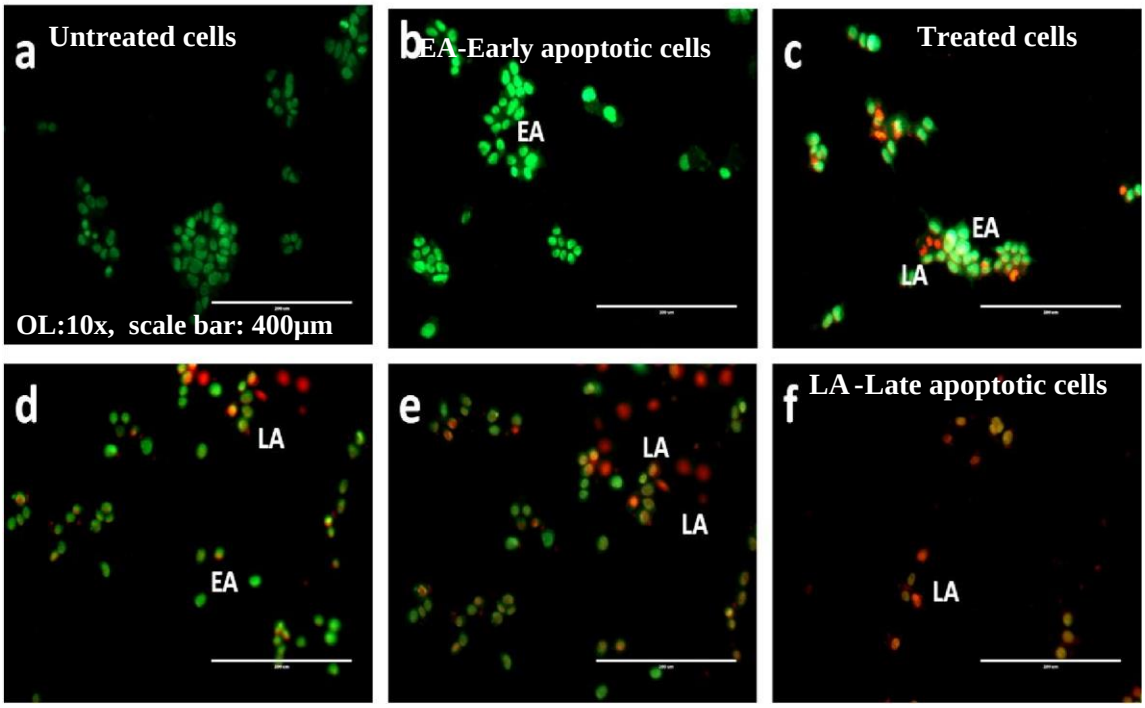

Fig. 9. *AO/EB stained images of (a) untreated cells, (b) - (f) NIR irradiated and cells treated with various concentrations of branched Au NPs (5 µg/mL, 10 µg/mL and 25 µg/mL) whereas EA in the image denotes early apoptotic cells and LA denotes late apoptotic cells (Objective lens 10x and scale bar: 400µm).*

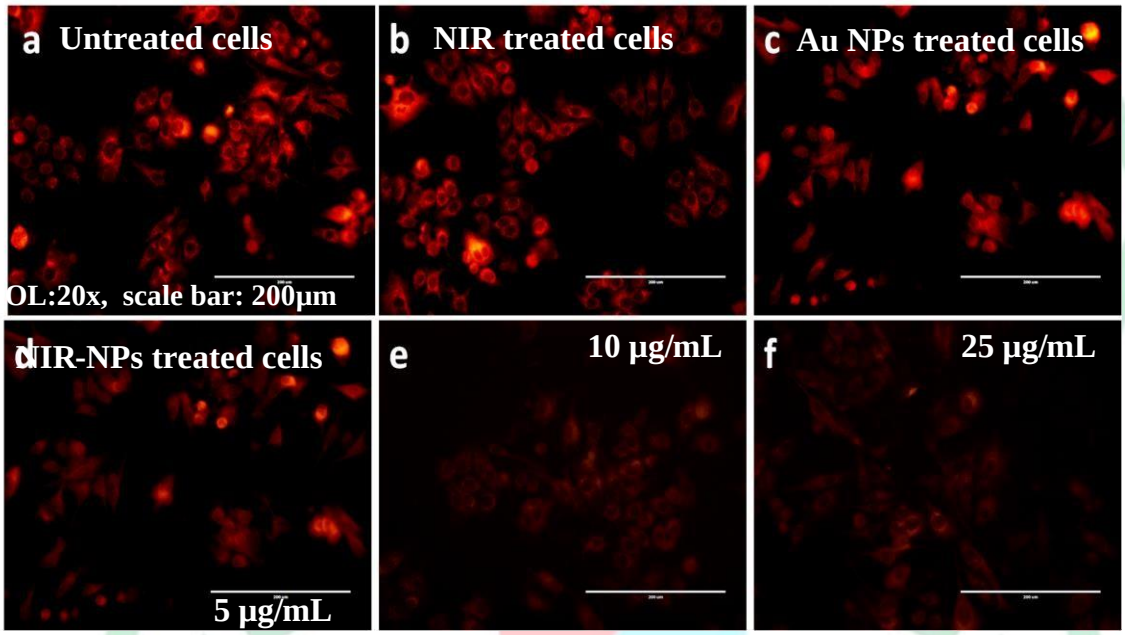

Fig. 10. *Fluorescence microscopic images of rhodamine 123 stained (a) untreated, (b) NIR treated, (c) branched Au NPs treated, and (d) - (f) NIR irradiated and various concentrations (5 µg/mL, 10 µg/mL and25 µg/mL) of branched Au NPs treated cells (Objective lens: 20 x and scale bar : 200 µm). The decline in the fluorescence of rhodamine 123 dye from control cells represents the depletion in mitochondrial membrane potential (MMP).*

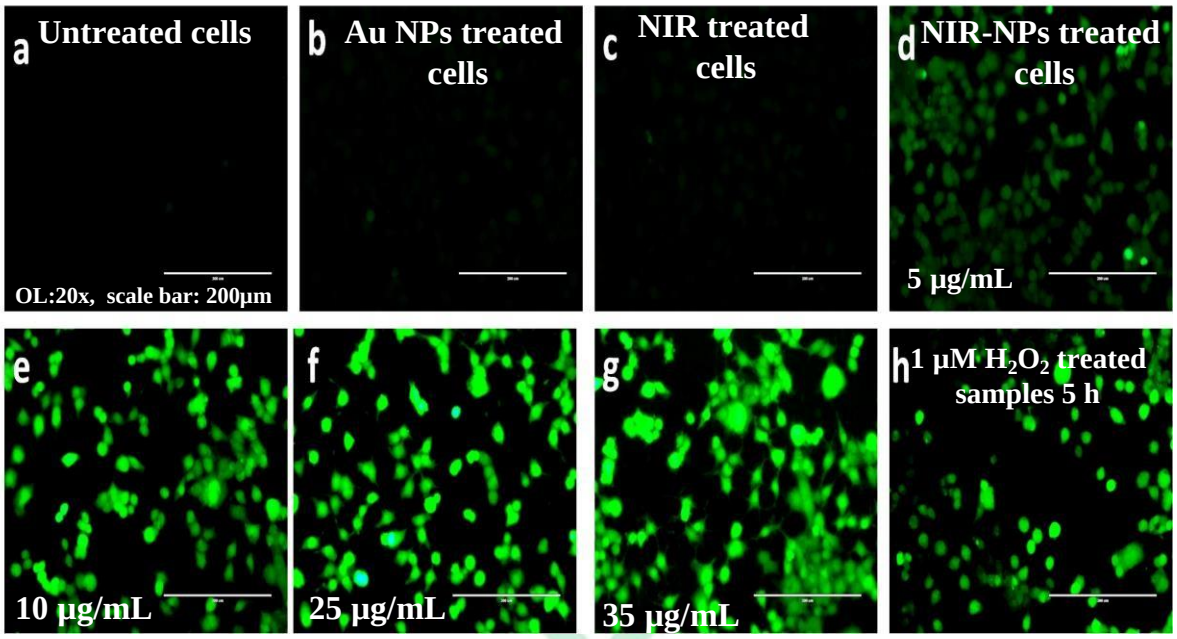

Fig. 11. *The fluorescent microscopic images depicting the level of intracellular ROS generation in various untreated and treated samples by DCF-DA dye based fluorescence intensity generation in (a) control cells, (b) only branched Au NPs treated, (c) only NIR treated, and (d) - (g) treatment with various concentration of branched Au NPs (5*

µg/mL, 10 µg/mL, 25 µg/mL and 35 µg/mL) followed by NIR exposure for 6 h, h) 1 µM H_2O_2 treated samples for the period of 5 h. (Objective lens: 20 x and scale bar : 200 µm).

Moreover, exposure to elevated temperatures causes harm to protein structures, including denaturation and the rupture of cell membranes, which may also lead to heightened oxidative stress.[36] Consequently, in light of the aforementioned discoveries, we propose that mitochondria may serve as a focal point for photothermal therapy, in addition to other organelles such as lysosomes. As a result, any harm inflicted on these components, along with the disruption of proteins and cellular membrane structures, could disrupt the oxidative equilibrium within cells, leading to the generation of reactive oxygen species (ROS).

4. Conclusions

This paper discusses the synthesis of gold nanoparticles of diverse sizes and shapes, achieved in an aqueous solution via a one-pot preparation technique utilising acetanilide and its derivatives at a temperature of 95 °C. These molecules serve dual purposes as reducing and structural agents, facilitating the creation of branched, multi-branched, and spherical gold nanostructures. The substitution at the para positions in acetanilide, including p-hydroxy and p-aminoacetanilide, results in the formation of both spherical and multi-branched gold nanoparticles. In contrast, acetanilide alone produces well-defined branched gold nanostructures exclusively. Consequently, the resulting branched gold nanoparticles can be effortlessly separated and refined without the need for complex purification methods. Fascinatingly, these branched gold nanostructures exhibited enhanced structural stability over the course of a year when compared to acetanilide derivatives that facilitated branched and multi-branched gold nanostructures. The branched gold nanoparticles exhibit robust surface plasmon resonance absorption within the near-infrared spectrum. Our experimental findings suggest that acetanilide-stabilized branched gold nanoparticles demonstrated superior photostability in comparison to its derivative-stabilized gold nanostructures. The efficiency of photothermal transduction reached an impressive 62.8% when exposed to an 808 nm laser diode, significantly surpassing that of other gold nanostructures and composite materials. Specifically, in vitro studies demonstrate that the branched gold nanostructures exhibit minimal cytotoxic effects, while effectively facilitating photothermal ablation of breast cancer cells when exposed to an 808 nm NIR laser.

References

[1]. Mirkin, C. A.; Letsinger, R. L.; Mucic, R. C.; Storhoff, J. J. *Nature* **1996**, *382*, 607-609.
[2]. Keating, C. D.; Kovaleski, K. M.; Natan, M. J. *J. Phys. Chem. B* **1998**, *102*, 9404-9413.
[3]. Jain, P. K.; Huang, X.; El-Sayed, I. H.; and El-Sayed, M. A. *Acc. Chem. Res*. **2008**, *41*, 1578-158
[4]. Ye, E.; Regulacio, M. D.; Zhang, S. Y.; Loh, X. J.; Han, M. Y. *Chem. Soc. Rev*. **2015**, *44*, 6001-6017.
[5]. Siegel, A. L.; Baker, G. A. *Nanoscale Adv.*, **2021**, *3*, 3980-4004.
[6]. Ortiz-Castillo, J. E.; Gallo-Villanueva, R. C.; Madou, M. J.; Perez-Gonzalez, V. H. *Coord. Chem. Rev*. **2020**, *425*, 213489.
[7]. Langer, J.; Jimenez De Aberasturi, D.; Aizpurua, J.; Alvarez-Puebla, R. A.; Auguie, B.; Baumberg, J. J.; Bazan, G. C.; Bell, S. E. J.; Boisen, A.; Brolo, A. G.; J. Choo; Cialla-May,
[8]. D.; Deckert, V.; Fabris, L.; Faulds, K.; Garcia de Abajo, F. J.; Goodacre, R.; Graham, D.; Haes, A. J.; Haynes, C. L. et al. *ACS Nano*, **2020**, *14*, 28-117.
[9]. Kim, D. Y.; Yu, T.; Cho, E. C.; Ma, Y.; Park, O. O.; Xia, Y. *Angew. Chem., Int. Ed.*, **2011**, 50, 6328-6331.
[10]. Kuttner, C.; Mayer, M.; Dulle, M.; Moscoso, A.; Lopez-Romero, J. M.; Forster, S.; Fery, A.; Perez-Juste, J.; Contreras-Caceres, R. *ACS Appl. Mater. Interfaces.* **2018**, *10*, 1115211163.
[11]. Jana, N. R.; Gearheart, L.; Murphy, C. J. *AdV. Mater.* **2001**, *13*, 1389-1393.
[12]. Wu, H. L.; Chen, C. H.; Huang, M. H. *Chem. Mater*., **2009**, *21*, 110-114.
[13]. Yuan, H.; Ma, W.; Chen, C.; Zhao, J.; Liu, J.; Zhu, H.; Gao, X. *Chem. Mater*., **2007**, *19*, 1592-1600.
[14]. Jena, B. K.; Raj, C. R. *Chem. Mater.* **2008**, *20*, 3546-3548.
[15]. Xie, J. P.; Lee, J. Y.; Wang, D. I. C. *Chem. Mater.* **2007**, *19*, 2823-2830.
[16]. Bakr, O. M.; Wunsch, B. H.; Stellacci, F. *Chem. Mater.* **2006**, *18*, 3297-3301.
[17]. Thambi, V.; Kar, A.; Ghosh, P.; Paital, D.; Gautam, A. R. S.; Khatua, S. *ACS Omega* **2019**, *4*, 3733-13739.
[18]. Sasidharan, S.; Bahadur, D.; Srivastava, R. *ACS Sustain. Chem. Eng.* **2017**, *5*, 10163- 10175.
[19]. Ahmed Al-Thabaiti, S.; Obaid, A. Y.; Khan, Z. *Can. Chem. Trans.* **2015**, *3*, 12-28.
[20]. Rajkumari, J.; Meena, H.; Gangatharan, M.; Busi, S. *IET Nanobiotechnol.* **2017**, 11, 987994.

[21]. Paul Reddy, K.; Jaiswal, K.; Satpati, B.; Selvaraju, C.; Murugadoss, A. *New J. Chem*. **2017**, *41*, 11250-11257.
[22]. Nehl, C. L.; Hafner, J. H. *J. Mater. Chem*. **2008**, *18*, 2415-2419.
[23]. Murugadoss, A.; Chatopadhyay, A. *J. Phys. Chem. C* **2008**, *112*, 11265-11271.
[24]. Marjanovic, C. G.; Marjanovic, B.; Bober, P.; Rozlivkova, Z.; Stejskal, J.; Trchova, M.; Prokes, J. *J. Polym. Sci., Part A: Polym. Chem.* **2011**, *49*, 3387-3403.
[25]. Roper, D. K.; Ahn, W.; Hoepfner, M. *J. Phys.Chem. C* **2007**, *111*, 3636-3641.
[26]. Li, X. G.; Huang, M. R.; Duan, W.; Yang, Y.L. *Chem. Rev.* **2002**, *102*, 2925-3030.
[27]. Li, X. G.; Huang, M. R.; Chen, R. F.; Jin, Y. Yang, Y. L. *J. Appl. Polym. Sci.* **2001**, *81*, 3107-311
[28]. Min, Y. L.; Wang, T.; Zhang, Y. G.; Chen, Y. C. *J. Mater. Chem.* **2011**, *18*, 6683-6689.
[29]. Pattani, V. P.; Shah, J.; Atalis, A.; Sharma, A; Tunnell, J. W. *J. Nanopart Res.* **2015**, *17*, 1-11.
[30]. Abadeer, N. S.; Murphy, C. J. *J. Phys. Chem. C* **2016**, *120*, 4691-471
[31]. Chen, C. L.; Kuo, L. R.; Chang, C. L.; Hwu, Y. K.; Huang, C. K.; Lee, S. Y.; Chen, K.; Lin, S. J.; Huang, J. D.; Chen, Y. Y. *Biomaterials* **2010**, *14*, 4104-4112.
[32]. Dubey, P.; Gopinath, P. *J. Mater. Chem. B* **2016**, *4*, 726-742.
[33]. Mocan, T.; Matea, C. T.; Cojocaru, I.; Ilie, I.; Tabaran, F. A.; Zaharie, F.; Iancu, C.; Bartos, D.; Mocan, L. *J Cancer*. **2014**, *5*, 679-688.
[34]. Wang, L.; Liu, Y.; Li, W.; Jiang, X.; Ji, Y.; Wu, X.; Xu, L.; Qiu, Y.; Zhao, K.; Wei, T.; Li, Y. *Nano Lett*. **2011**, *11*, 772-780.
[35]. Dubey, P.; Gopinath, P. *J. Mater. Chem. B* **2016**, *4*, 726-742.
[36]. Markovic, Z. M.; Harhaji-Trajkovic, L. M.; Todorovic-Markovic, B. M.; Kepic, D. P.; Arsikin, K. M.; Jovanovic, S. P.; Pantovic, A. C.; Dramicanin, M. D.; Trajkovic, V. S. *Biomaterials* **2011**, *32*, 1121-1129.
[37]. Jaque, D.; Maestro, L. M.; Del Rosal, B.; Haro-Gonzalez, P.; Benayas, A.; Plaza, J. L.; Rodriguez, E. M.; Sole, J. G. *Nanoscale*, **2014**, *6*, 9494-9530.